Strain and Piezo-Doping Mismatch between Graphene Layers

Alexis Forestier, Félix Balima, Colin Bousige, Gardênia de Sousa Pinheiro, Rémy Fulcrand, Martin Kalbáč, Denis Machon, Alfonso San-Miguel

Strain and Piezo-doping Mismatch Between Graphene Layers

A. Forestier,[†] F. Balima,[†] C. Bousige,[*,‡] G. de Sousa Pinheiro,[†,¶] R. Fulcrand,[†] M. Kalbáč,[§] D. Machon,[*,†,‖] and A. San-Miguel[*,†]

[†]*Univ Lyon, Université Claude Bernard Lyon 1, CNRS UMR 5306, Institut Lumière Matière, F-69622 Villeurbanne, France*

[‡]*Univ Lyon, Université Claude Bernard Lyon 1, CNRS UMR 5615, Laboratoire des Multimatériaux et Interfaces, F-69622 Villeurbanne, France*

[¶]*Departamento de Física, Campus Ministro Petrônio Portella, Universidade Federal do Piauí, CEP 64.049-550 Teresina, PI, Brazil*

[§]*Heyrovský Institute of Physical Chemistry of the Czech Academy of Sciences, v.v.i., Dolejškova 2155/3, Czech Republic*

[‖]*Laboratoire Nanotechnologies et Nanosystèmes (LN2), CNRS UMI-3463, Université de Sherbrooke, Institut Interdisciplinaire d'Innovation Technologique (3IT), Sherbrooke, Québec, Canada*

E-mail: colin.bousige@univ-lyon1.fr; denis.machon@univ-lyon1.fr; alfonso.san-miguel@univ-lyon1.fr

Abstract

Modulation of electronic properties of bilayer materials through the strain and doping mismatch between layers opens new opportunities in 2D-materials straintronics. We present here a new approach allowing to *generate* asymmetric strain or doping between layers, and a method to *quantify* it using supported isotopically labeled bilayer graphene studied by *in situ* Raman spectroscopy. Strain differences up to $\sim 0.1\%$ between the two graphene layers have been obtained by applying pressures up to 10 GPa with non-polar solid environments. However, when immersed in a liquid polar environment, namely a mixture of ethanol and methanol, a piezo-doping mismatch between layers is observed. This asymmetrical doping increases with pressure, leading to charge concentration differences between layers of the order of 10^{13} cm^{-2}. Our approach thus allows disentangling strain and doping effects in high pressure experiments evidencing the asymmetries of these phenomena and comforting isotopic bilayer graphene as a benchmark system for the study of asymmetric effects in devices or composite surfaces.

Introduction

Fine-tuning the electronic properties of graphene and other 2D-systems is at the forefront of both fundamental and applied research in nanoscience and nanotechnology. Two commonly methods used in view of the optimization of 2D-systems properties are doping and strain application.[1,2] In bilayer graphene asymmetrical doping or strain, *i.e.* a different doping level for the two graphene layers, has been explored as a function of the system temperature[3] and it has been predicted that such asymmetry should depend on the twist angle.[4] Asymmetrical doping or strain has never been observed in the study of bilayer graphene submitted to high mechanical constraints. In this work we

show that such asymmetries can be extraordinary important in supported bilayer graphene submitted to high pressures. Such asymmetries need to be considered to correctly interpret experiments and we show how to quantify them. The observed effects offer new opportunities for the developments of an *asymmetric straintronics* able to modulate electronic properties taking advantage of induced asymmetries between 2D-system layers.

Here, we have studied supported isotopically-labeled bilayer graphene (BLG) using Raman spectroscopy under high pressure conditions. Raman spectroscopy is a very powerful technique allowing probing both mechanical and chemical perturbations.[5–8] The use of isotopically labeling is interesting as it allows separating the Raman signal of the top graphene layer (in contact with its environment) from the one of the bottom graphene layer – in contact with the substrate and supposedly screened from the interaction with the environment.[9,10] Combining isotopically labeled BLG with Raman spectroscopy has proven to be particularly useful to explore the effect of the sample environment.[11]

In high pressure experiments, by submitting the whole supported 2D-system to high pressures, it is possible to explore a large domain of compressive biaxial strain due to the volume reduction of the substrate on which the 2D system lays.[2,12–14] This biaxial strain is then transmitted to the bottom graphene layer laying on the substrate. At the same time, pressure also enhances any potential chemical interaction between the surrounding media and the top layer. Consequently, the isotopic selectivity in BLG would not only allow measuring mechanical or chemical effects on the system, but also any mismatch of these effects between the two graphene layers. Pressure application allows progressively increasing strain and chemical interactions with the isotopically labeled 2D-system and thus constitutes a benchmark application to separate chemical and mechanical effects as well as spectroscopic signatures. This separation of effects between the 2D-system layers can be compared to the analogous separation between mechanical and chemical response in double-walled carbon nanotubes, probed in high pressure experiments.[15,16]

In this work, we have studied the pressure response of supported BLG immersed in three different media: argon and nitrogen, which are supposedly non-doping media, and a 4:1 methanol:ethanol mixture. When using water or alcohol as pressure transmitting media (PTM), there has been a number of claims of chemical effects, doping or covalent functionalization, associated to strain ones,[5,17,18] while other studies show no evidence of such effects for experiments in similar conditions.[2,12,19]

By exploring the pressure evolution of the Raman signal, our work not only shows that the alcohol PTM leads to a piezo-doping effect, but also allows measuring and characterizing doping and strain mismatches between the two layers. Such differences allows exploring new paths for the straintronics tuning of the opto-electronic properties of graphene-based devices and composites.[20]

Experimental

BLG was produced from two independent chemical vapor deposition (CVD) growths on copper substrate, using either $^{12}CH_4$ or $^{13}CH_4$ as precursors. The obtained ^{12}C and ^{13}C isotopically-labeled graphene layers are then transfered on a Si/SiO_2 silicon substrate (50 μm Si thickness covered with a 300 nm SiO_2 layer), with ^{12}C graphene on the bottom and ^{13}C graphene on the top (Fig. 1(a)). Details on the synthesis and transfer method on the Si/SiO_2 substrate are given in reference.[21] Raman profiles at ambient pressure clearly indicate that our samples are turbostratic.[22] The twist angle between layers cannot be determined due to the polycrystalline nature of both graphene layers combined with high pressure experimental constraints.

Pieces of SiO_2/Si substrate (side $\sim$ 40 μm) supporting the BLG sample were cleaved and placed in the diamond anvil cell (DAC) which allows generating multi-GPa range pressures. The fluorescence of a small ruby was used for pressure calibration.[23] Three differ-

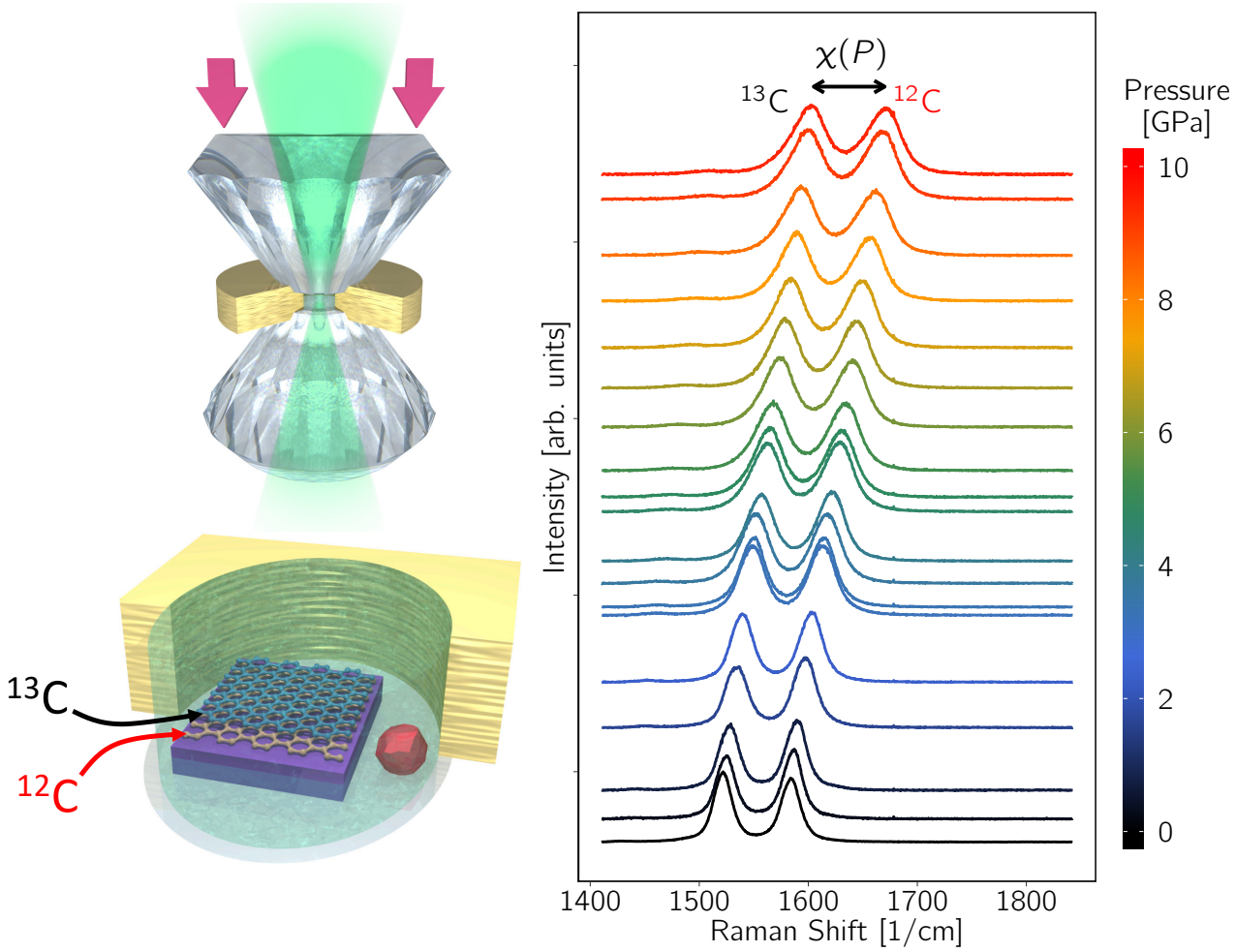

(a) (b)

Figure 1: (a) Experimental set-up used in the Raman experiments showing the sample loaded in the diamond anvil cell. The applied force (red arrows) on the diamonds compresses the experimental cavity delimited by the two diamonds and a metallic gasket – opened to show the sample volume. The laser light illuminates the sample and the Raman signal is collected in backscattering mode. The sample volume is shown below and consists in a supported isotopically-labeled BLG immersed in a PTM. A ruby chip (red crystal) is used for *in situ* pressure calibration. (b) Evolution of the Raman G-bands of isotopically-labeled BLG as a function of pressure using nitrogen PTM. The spectra are background corrected and normalized to the G-band height, and the baseline height corresponds to the applied pressure (right axis). $\chi(P)$ is the difference between G-bands positions.

ent PTM were used: argon, nitrogen and a 4:1 methanol:ethanol mixture. All PTM were loaded in their liquid state. While all three PTMs are considered as providing hydrostatic or quasi-hydrostatic conditions in the 0–10 GPa range,[24] only the alcohol mixture remains liquid (and thus perfectly hydrostatic) over this whole pressure range – argon and nitrogen crystallize around 1.15 GPa and 2.4 GPa, respectively.[25–27] Pressure application was controlled by a deformable membrane applying the driving force on the DAC piston.[28] Finally, we note that at ~ 11 GPa the silicon substrate follows a phase transformation towards its tetragonal β-Sn phase with a 21 % volume reduction,[29] leading to substrate damage and usually signal loss.

The Raman spectra were recorded using two LabRAM HR spectrometers (Horiba Jobin Yvon) and a homemade Raman set-up. The excitation laser line was 2.33 eV (532 nm) for nitrogen and alcohol PTM experiments and 2.41 eV (514.5 nm) for the argon PTM measurements. In all cases, the scattered light was collected in back-scattering geometry through the diamond anvil with a long-working distance objective (50× magnification with numerical aperture between 0.4 and 0.5 depending on the set-up used). The spectral resolution is ~ 1 cm^{-1}. We cannot observe the *in-situ* D-band evolution as it is masked by the prominent F_{2g} diamond Raman peak up to at least 15 GPa.[30] The experimental set-up is sketched in Fig. 1(a) with more details available in the Supplementary Information (SI).

Results

Fig. 1(b) shows the Raman spectra of the isotopically labeled-BLG at different pressures using nitrogen as PTM. Differences between the raw spectra using the different PTM are difficult to appreciate without further analysis. Raw spectra for argon and the alcohol mixture PTM are nevertheless presented in SI. The two visible peaks correspond to the G-band for each isotopically-labeled layer, with the ^{12}C bottom layer at $\omega_G^{bot} \simeq 1582$ cm^{-1}, and the ^{13}C top layer at $\omega_G^{top} = \sqrt{12/13} \times \omega_G^{bot} \simeq 1520$ cm^{-1} at ambient pressure. The two peaks blue-shift with pressure increase, and their positions and width could be extracted by fitting either with Lorentzian or Voigt functions (see SI for details). We define the difference in G-band positions between the two layers, $\chi(P) = \omega_G^{bot}(P) - \omega_G^{top}(P)$.

The fitted G-band shifts as a function of pressure, $\Delta\omega_G(P) = \omega_G(P) - \omega_G(0)$, are gathered in Fig. 2.(a) for the three PTM. In graphene, the G-band position is very sensitive to the strain in the system, but also to electron concentration changes (electron or hole doping) through electron-phonon coupling.[7] The representation $\Delta\omega_G(P) = \omega_G(P) - \omega_G(0)$ allows comparing different experiments.

In our experimental set-up, the BLG sample is submitted to a compressive biaxial strain due to the volume reduction of the substrate, *i.e.* $\varepsilon = \varepsilon_{xx} = \varepsilon_{yy}$ (no shear strain).[12] Therefore, the shift of the optical phonons as a function of the biaxial strain reduces to $\Delta\omega_s = -2\gamma_s\omega_s^0\varepsilon$, where $\Delta\omega_s$ is the strain-induced shift of the s phonon mode s, ω_s^0 its frequency at zero strain, and γ_s its Grűneisen parameter.[31] Consequently, for purely mechanical response, the Raman shift evolution is directly proportional to the sample's strain. It also depends on the isotopic weight through the ω_0 term.

The black solid line in Fig. 2.(a) represents the expected G-band shift for the bottom layer in the ideal case of a total strain transfer from the substrate. This line is calculated using the high-pressure range of the silicon equation of state given in reference[32] and the G-band Grűneisen parameter $\gamma_G = 1.8$ – the latter being deduced from measurements on mono-layer graphene biaxially strained at high pressure in perfect adhesion on diamond.[2,12] Fig. 2.(a) shows that, in all cases, the data points are below this ideal line, meaning that the deformation of the substrate is never fully transmitted to the BLG: we thus expect local buckling, wrinkling, and sliding of the graphene, resulting in an inhomogeneous strain field in the sample.[2,12] This in turn results into the G-band full width at half maximum (FWHM) increase with pressure (Fig. 2.(c)). The black dashed line in

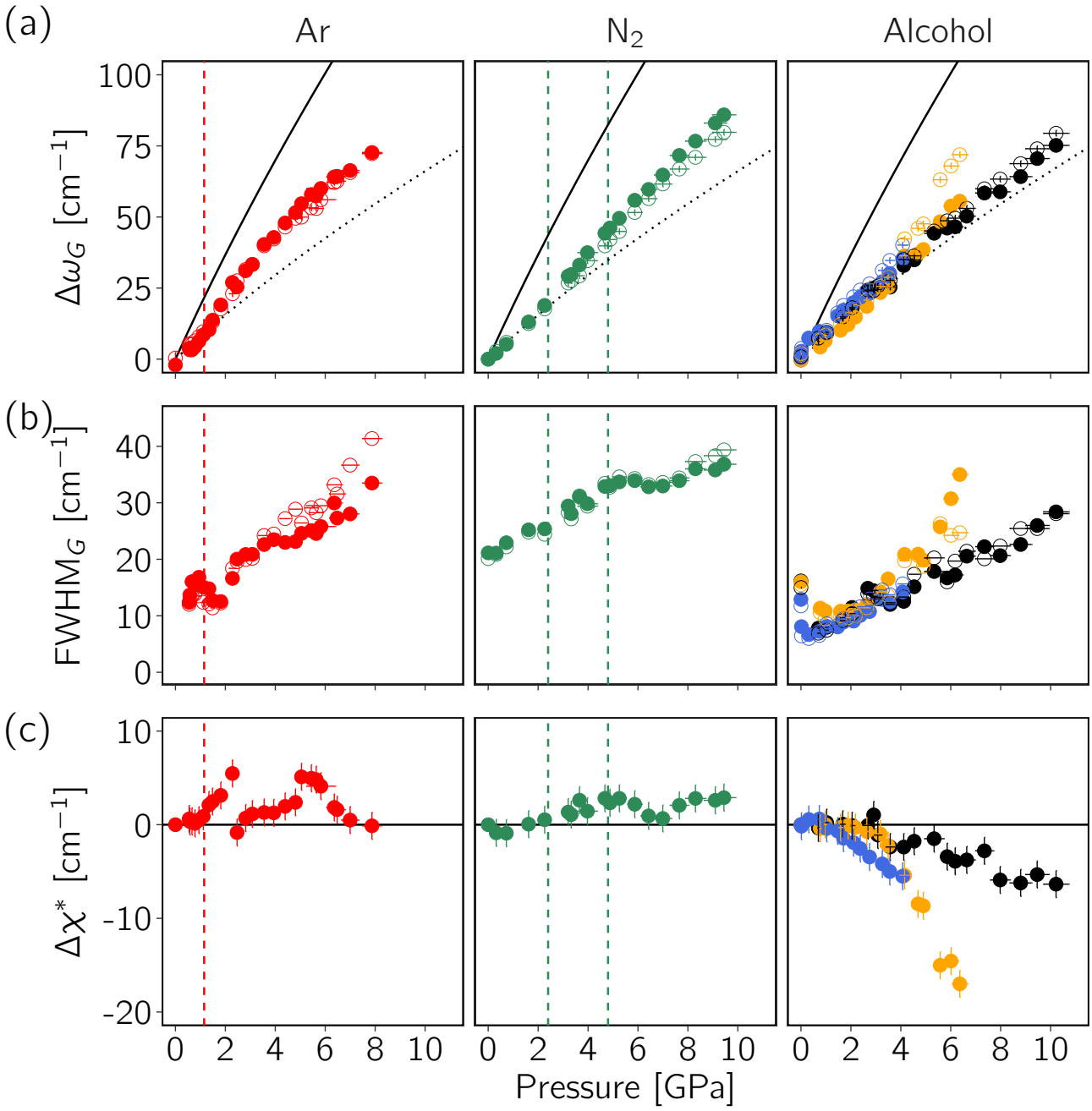

Figure 2: Pressure evolution of the G-band shifts (a) and FWHM (b), for the top (empty symbols) and bottom (full symbols) graphene layers in argon, nitrogen and in a 4:1 methanol:ethanol mixture (alcool). Panel (c) shows the corrected G-band shift difference between the graphene bottom and top layers, $\Delta\chi^* = \Delta\omega_G^{bot} - \sqrt{13/12} \times \Delta\omega_G^{top}$ – where the $\sqrt{13/12}$ term allows correcting for the isotope weight difference. When using alcohol PTM (right column), three different experiments are presented. In panel (a), the expected ideal evolution in the case of perfect adhesion of the sample on substrate is plotted for the bottom layer as a black solid line. The black dashed line in (a) corresponds to the extrapolation of the low pressure data points for nitrogen and argon (before solidification), also shown for comparison in the alcohol case. PTM solidification and crystalline phase transitions pressures are indicated by vertical lines at 1.15 GPa for argon, and 2.4 GPa and 4.8 GPa for nitrogen.[25–27] Vertical error bars are given by the fit standard error when larger than spectral resolution. Pressure error bars are estimated at 5 % of the measured pressure.

Fig. 2.(a) is the extrapolation of the low pressure – *i.e.* liquid PTM – G-band evolution for nitrogen and argon PTM. It is plotted considering a strain transfer efficiency of $\sim 42\%$ from the substrate to graphene, deduced from the liquid PTM pressure points for the two layers. This projected evolution is also shown in the alcohol PTM case in Fig. 2.(a) for the sake of comparison.

Fig. 2.(c) shows the pressure evolution of the G-band shift difference between the two graphene layers corrected for the isotopic weight, $\Delta\chi^* = \Delta\omega_G^{bot} - \sqrt{13/12} \times \Delta\omega_G^{top}$. In the hypothesis where the BLG response is purely mechanical, we then have $\Delta\chi^*(P) \propto |\varepsilon^{bot}(P)| - |\varepsilon^{top}(P)|$. The evolution of $\Delta\chi^*(P)$ in Fig. 2.(c) shows two opposite behaviors depending on the PTM nature: for the argon and nitrogen cases, the bottom layer has its G-band more blue-shifted than the bottom layer ($\Delta\chi^* > 0$), while we observe the opposite trend in the case of alcohol PTM.

Finally, Fig. 2.(b) presents the pressure evolution of the G-bands FWHM for the different experiments. As a global trend, the G-band FWHM increases with pressure application for all PTMs, as expected for an increasing inhomogeneous strain field in the sample. However, for the alcohol PTM, in the very low pressure regime there is a strong drop in the G-band FWHM – roughly 5 cm^{-1} to 10 cm^{-1} depending on the experiment – that cannot be explained by a purely mechanical response.

Discussion

In this section, we will split the discussion between results obtained with (i) argon and nitrogen PTMs, for which the response is governed by pure mechanical effects; and (ii) results for the alcohol mixture PTM, which, as it will be seen, exhibits a prominent piezo-doping effect.

Strain mismatch between layers

We restrain our discussion in this section to the argon and nitrogen PTM cases. In graphenic systems, a shift of the G-band can arise from (i) elastic strain, and/or (ii) a modification of the carrier concentration in the graphene layer. The $\Delta\omega_{2D}$ vs. $\Delta\omega_G$ correlation diagram is commonly used to decorrelate strain and doping in graphene Raman scattering experiments.[33,34] In our case, for nitrogen PTM we obtain values of $\partial\omega_{2D}/\partial\omega_G = 2.47 \pm 0.03$ for the top layer and 2.33 ± 0.03 for the bottom layer. In the argon PTM case, we obtain $\partial\omega_{2D}/\partial\omega_G = 2.31 \pm 0.09$ and 2.14 ± 0.05 for the top and the bottom layer, respectively. All these values are close to the reported value for pure biaxial strain in single layer graphene, $\partial\omega_{2D}/\partial\omega_G = 2.2 \pm 0.2$[7] (see details in SI). As a consequence, the data for nitrogen and argon PTM can safely be interpreted as a purely mechanical response to the applied pressure.

The black dashed line in Fig. 2.(a) corresponds to the expected projection of the biaxial strain if it was transmitted by the sole substrate to the bottom layer. Fig. 2.(a) shows that, even after PTM solidification, all data-points are relatively close to the dashed line, which indicates that the substrate-induced biaxial compression is the dominant effect determining the observed Raman response. Nevertheless, after PTM solidification the data-points evolution is higher than the dashed line extrapolation, which is the signature of an additional stress from the solid PTM. These findings are in very good agreement with similar experiments with argon PTM performed on exfoliated non-isotopically labeled bilayer graphene.[2]

Fig. 2.(c) shows that in the solid PTM domain $\Delta\chi^*(P) > 0$ for argon and nitrogen, *i.e.* the solidification of the PTM results in a differentiation of the layers response. As $|\varepsilon^{bot}| > |\varepsilon^{top}|$, despite of the larger compressibility of the solid PTM, we conclude that the strain transfer from the solid PTM is much weaker than from the substrate. This is then explained by a weaker overall adhesion of BLG on the solid PTM.

We observe a number of accidents in the evolution of $\Delta\chi^*(P)$ and in the G-band FWHM (Fig. 2.(b-c)). These events can be associated with the discontinuous transformations of the PTM. For nitrogen, we can highlight its crystallization at ~ 2.4 GPa and the hexagonal to cubic phase transformation at ~ 4.8.[27] For argon,

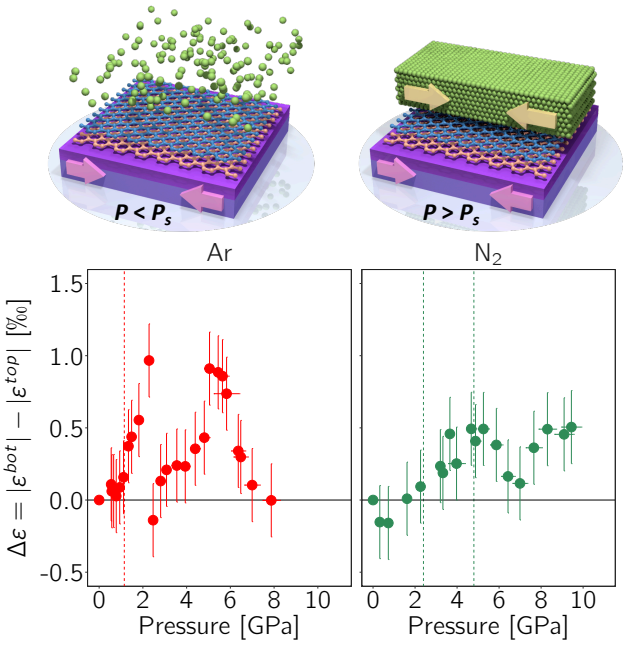

Figure 3: Strain difference $|\varepsilon^{bot}| - |\varepsilon^{top}|$ between the two graphene layers as function of pressure for argon and nitrogen as PTM. Values are given in ‰. On top are shown schematically the two situations of the sample when the PTM is liquid ($P < P_s$) and when it is solid ($P > P_s$). The solidification pressure, P_s, corresponds to the first vertical dashed lines in both graphs.

we should underline its crystallization around 1.2 GPa, its hydrostaticity limit at $\sim$ 1.9 GPa[35] and its known recrystallizations at higher pressures.[25,36,37] These changes in the vicinity of the BLG surface should reflect strain variations or relaxations in the system, leading to the observed anomalies. Measuring the strain difference between the two graphene layers of an isotopically labeled BLG system using Raman spectroscopy thus appears as an *extremely* sensitive probe of the mechanical characteristics of different PTMs. In fact, our results are in quantitative agreement with the PTM hydrostaticity limits of reference.[35]

It is worth quantifying the strain difference between the two layers. This calculation is straightforward since the strain difference is proportional to $\Delta\chi^*$ through the relation $|\varepsilon^{bot}| - |\varepsilon^{top}| = \Delta\chi^*(P)/\left[2\gamma_G\omega_G^{bot}(P=0)\right]$. The pressure evolution of the strain difference is presented in Fig. 3.

At its maximum, this difference is $|\varepsilon^{bot}| - |\varepsilon^{top}| \simeq 0.1\%$ for argon PTM, $\simeq 0.05\%$ in the case of nitrogen PTM. Consistently, in a study of isotopically labeled BLG directly compressed between two sapphire crystals,[38] *i.e.* $|\varepsilon^{bot}| - |\varepsilon^{top}| = 0$, $\Delta\chi$ remained zero during the whole compression experiment. Some of the differences between the two experiments may arise from different mechanical coupling of the two graphene layers associated with differences in the twist-angle.

Piezo-doping effects

In this section we discuss our results when using the 4:1 methanol:ethanol mixture as PTM. This mixture remains liquid up to its glass transition at 10.5 GPa,[24] we may then expect similar results to the argon and nitrogen PTMs in their liquid phase. It is not the case as for alcohol PTM, $\Delta\chi^*(P) < 0$ in the whole pressure range (Fig. 2.(c)). The $\Delta\chi^*(P) < 0$ observation suggests that the BLG response to high-pressure application is not purely mechanical. In the case of alcohol PTM, the 2D-bands signal could not be observed or only as a very weak signal at low pressures, not allowing its use for doping characterization (for more details, see SI).

It was shown that both n and p doping induce a blue-shift of the Raman G-band, a narrowing of its FWHM and the 2D-band intensity attenuation.[7,39–45] These three effects are observed in all our experiments using alcohol PTM, in favor of a pressure induced doping effect. Indeed, (i) the G-bands blue-shift on Fig. 2.(a) is stronger than the dashed line extrapolation for liquid PTM when pressure increase, (ii) a strong G-band FWHM drop (equivalent for both layers) is observed at the beginning of the compression, and (iii) the 2D-bands signal disappeared at very low pressure (see details in SI).

Since $\Delta\omega_G$ increases with doping, $\Delta\chi^*(P)$ for the alcohol PTM probes the difference in charge carrier concentration between the two graphene layers. For all experiments, Fig. 2.(c) shows that $\Delta\chi^*(P) < 0$ with a monotonous decrease, meaning that the top layer is more doped than the bottom one, and that this difference increases with pressure. Such pressure-induced increase in the difference of charge concentra-

tion is expected. Indeed, the graphene surface exposed to the alcohol PTM is the most susceptible to interact with it, and this interaction is increased by the pressure-induced reduction in PTM-graphene distance. Such asymmetrical doping has already been observed in gate induced doping experiments on twisted bilayer graphene immersed in an ion gel electrolyte.[46]

From the $\Delta\omega_G(P)$ evolution, it is possible to roughly evaluate the carrier concentration of each layers with alcohol PTM. Considering the black dashed line extrapolation on Fig. 2.(a) as the pure mechanical contribution to the G-bands shift, $\Delta\omega_G^{mech}(P)$, the doping-induced Raman shift $\Delta\omega_G^{dop}(P) = \Delta\omega_G(P) - \Delta\omega_G^{mech}(P)$ can be translated in terms of charge carrier concentration through the DFT models proposed by Lazzeri *et al.* either using LDA/GGA[41] or GW[47] functionals to evaluate the electron-phonon coupling. Such type of approaches have been successfully applied to determine the doping levels in chemically doped graphene and graphite intercalated systems.[44,48] We have calculated the charge carrier concentration difference between the two layers, $\Delta n = |n^{bot}| - |n^{top}|$ as function of pressure for our experiments using alcohol PTM. We have considered the two different models of Lazzeri *et al.*[41,47] accounting for a lattice parameter evolution arising solely from the biaxial strain partially transferred from the substrate[12] and not from doping due to substrate pinning.[44] The results are presented on Fig. 4, where one can appreciate that doping differences between layers of the order of 10^{13} cm^{-2} can be reached. In this graph we have considered the non-adiabatic contributions either using LDA/GGA[41] or GW approximations,[47] which define the shaded area in the Figure 4. Due to the high symmetry of the charge concentration in the low G-band Raman shift region (Fig. S7), it is not possible to discriminate from the sole combination of experiments and models between hole or electron doping.

It appears clearly in Fig. 2.(c) that the $\Delta\chi^*(P)$ difference is weaker in one of the alcohol PTM experiments (black symbols). This particular behavior may be explained due to the graphene-substrate unbinding[12] in this particular experiment leading to a lower value of $\Delta\omega_G^{mech}(P)$ (consistently with our data on Fig. 2.(a)). We have clearly observed pressure induced unbinding in experiments with thicker samples. Such partial unbinding would in turn involve a progressive exposure of the bottom graphene layer to the PTM and hence allow for the interaction of the PTM with the bottom layer too, leading to a reduction of the absolute value of $\Delta\chi^*(P)$ as observed. As $\Delta\omega_G^{mech}(P)$ is modified in this particular experiment with respect to all others, we can not evaluate its doping evolution with pressure and the corresponding points are not included in Fig. 4. Additionally, we note that the G-band FWHM for one of alcohol PTM experiments in Fig. 2(b) shows an anomalous high value, in particular for the bottom layer. We have systematically observed a progressive delamination of the oxide layer at $\sim$ 4-5 GPa in all alcohol PTM experiments (see SI for pictures), whereas it was absent for the argon or nitrogen PTM ones. This may be related

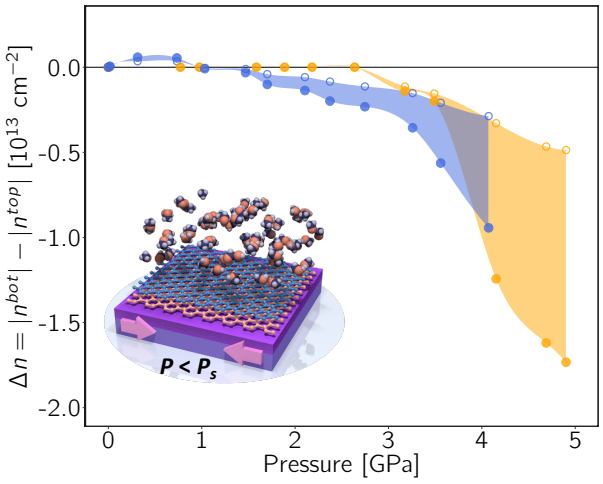

Figure 4: Charge carrier concentration difference $\Delta n = |n^{bot}| - |n^{top}|$ between the two graphene layers as function of pressure using alcohol PTM. Filled circles correspond to the evaluated values using the model of Ref.[47] for hole carriers and the empty ones to electrons with model of Ref.[41] The areas in between cover the other two combinations. The two colors corresponds to the two experiments in Fig. 2. The inset schematically shows the situation in the whole pressure domain where the alcohol PTM remains liquid.

to the well known favoured glass network breakdown by polar molecules.[49] To avoid such spurious contributions only data below that pressure domain has been considered for the charge carrier difference evaluation of Fig. 4. There is an overall good agreement between the two experiments in Fig. 4 with some differences which may arise from twist-angle dissemblance.

Values of $\partial\omega_G/\partial P$ were considered as a doping effect argument in an earlier work.[5] Nevertheless, subsequent works in references[2,12,19] showed the difficulties to use such parameter alone for doping characterization. Thanks to the use of isotopically-labeled BLG samples and through the observation of the inversion of the $\Delta\chi^*(P)$ evolution, we are able to disentangle doping and mechanical stress effects arising from the PTM.

Our work does not provide direct information on the piezo-doping mechanism associated with the use of alcohol PTM. Nevertheless we may discuss different possibilities. Pressure studies of bilayer graphene in water PTM have proposed the formation of sp^3 bonds on the top layer with -OH groups leading at the same time to an sp^3 hybridization between the two graphene layers, a transition observed around 5-10 GPa.[17,18] In our study, such a high-pressure onset hybridization hypothesis cannot be invoked since doping appears from the earliest pressure stages. Electronic doping of graphene by surface adsorbates[50] appears as a more favorable scenario. In fact, it has been shown that water, toluene or F4TCNQ, *i.e.*, polar molecules, show at ambient pressure such type of doping, whereas the non-polar molecule naphthalene, for instance, does not.[51] The dipolar nature of the molecule thus seems to be a factor favoring graphene electronic doping through surface adsorption. Pressure enhances the surface environment interaction and may lead to exalt such doping effect. We should nevertheless underline that the graphene doping mechanism associated with the adsorption of atoms or molecules may be complex including red-ox interactions mediated by the presence of other molecules[50] and may also be affected by the incident Raman laser power.[52] Asymmetrical doping of graphene layers in BLG through molecular doping has been additionally shown to lead to a gap opening:[53] for p-doping molecules containing π-electrons, the band gap is estimated to evolve as 40 meV/10^{13} cm^{-2}.

The extension of this type of pressure study to other molecular fluids known to electronically dope graphene at ambient conditions[51] could further enhance the piezo-doping effect, thus bringing interesting outcomes both from the fundamental point of view as well as for applications. Combining our approach with the study of unsupported samples[54,55] could allow to better explore the physico-chemical origin of piezo-doping effects.

Conclusions

Our work shows that the study of supported isotopically-labeled bilayer graphene at high pressure not only allows disentangling mechanical and chemical effects in a remarkable way but also evidence strong asymmetries. While the bottom layer is mechanically strained by the substrate compression, the top graphene layer can exchange chemically or mechanically with its environment. Experiments were done using three different pressure transmitting media: argon, nitrogen and 4:1 methanol:ethanol. We have shown that, as far as these media remain liquid, the measured mechanical strain is transferred from the substrate to the two layers of the system without asymmetry. Conversely, the solidification of the pressure medium leads to a slight decoupling of the layers, leading to a strain mismatch of up to 0.1 %. In the case of the 4:1 methanol:ethanol medium we have evidenced a remarkable piezo-doping effect on the graphene layer in contact with the alcohol molecules which remain in their liquid state. The piezo-doping is strongly asymmetrical, with the top layer showing a charge concentration of the order of 10^{13} cm^{-2} above the lower one.

Asymmetric doping or strain between layers can bring opportunities in band structure engineering of two-layer systems[4,53] with possible applications including devices or composite materials optimization, paving the way for the de-

velopment of *asymmetric straintronics*.

Acknowledgement

We thank Jérémie Margueritat (University Lyon 1) for advices and recommendations to upgrade one of the Raman spectrometers, and David Dunstan (Queen Mary University of London) for fruitful scientific discussion. This work has been done thanks to the support of the PLECE and CECOMO platforms of the University of Lyon. We acknowledge support from the iMUST LABEX program MUSCAT-2D. We thank also the French-Brazilian CAPES-COFECUB program through project Ph 938/19. We acknowledge financial support by COST project (LTC18039) and Ministry of Education, Youth and Sports of the Czech Republic and The European Union - European Structural and Investments Funds in the frame of Operational Programme Research Development and Education - project Pro-NanoEnviCz (Project No. CZ.02.1.01/0.0/0.0/16_013/0001821).

Supporting Information

Experimental details, Micrographs of samples at various pressures, data and fitting procedure, Raman spectra (G and 2D bands) in all experiments, Raman spectra after pressure cycle, Charge carrier concentration calculation details, 2D band evolution with pressure and Lee's diagram.

References

(1) Si, C.; Sun, Z.; Liu, F. Strain engineering of graphene: a review. *Nanoscale* **2016**, *8*, 3207–3217.

(2) Machon, D.; Bousige, C.; Alencar, R.; Torres-Dias, A.; Balima, F.; Nicolle, J.; de Sousa Pinheiro, G.; Souza Filho, A. G.; San-Miguel, A. Raman scattering studies of graphene under high pressure. *Journal of Raman Spectroscopy* **2018**, *49*, 121–129.

(3) Verhagen, T. G. A.; Drogowska, K.; Kalbac, M.; Vejpravova, J. Temperature-induced strain and doping in monolayer and bilayer isotopically labeled graphene. *Phys. Rev. B* **2015**, *92*, 125437.

(4) Trambly de Laissardière, G.; Namarvar, O. F.; Mayou, D.; Magaud, L. Electronic properties of asymmetrically doped twisted graphene bilayers. *Phys. Rev. B* **2016**, *93*, 235135.

(5) Nicolle, J.; Machon, D.; Poncharal, P.; Pierre-Louis, O.; San-Miguel, A. Pressure-Mediated Doping in Graphene. *Nano Letters* **2011**, *11*, 3564–3568.

(6) del Corro, E.; Kavan, L.; Kalbac, M.; Frank, O. Strain Assessment in Graphene Through the Raman 2D′ Mode. *The Journal of Physical Chemistry C* **2015**, *119*, 25651–25656.

(7) Bendiab, N.; Renard, J.; Schwarz, C.; Reserbat-Plantey, A.; Djevahirdjian, L.; Bouchiat, V.; Coraux, J.; Marty, L. Unravelling external perturbation effects on the optical phonon response of graphene: External perturbation effects on graphene optical phonons. *Journal of Raman Spectroscopy* **2018**, *49*, 130–145.

(8) Yang, K. L.; Lee, J. O.; Choo, H.; Yang, F. Can Raman Shift Be Used To Characterize the Mechanical Property of Graphene? *The Journal of Physical Chemistry C* **2018**, *122*, 24467–24474.

(9) Kalbac, M.; Kong, J.; Dresselhaus, M. S. Raman Spectroscopy as a Tool to Address Individual Graphene Layers in Few-Layer Graphene. *The Journal of Physical Chemistry C* **2012**, *116*, 19046–19050.

(10) Costa, S. D.; Weis, J. E.; Frank, O.; Fridrichová, M.; Kalbac, M. Addressing Raman features of individual layers in isotopically labeled Bernal stacked bilayer graphene. *2D Materials* **2016**, *3*, 025022.

(11) Ek Weis, J.; Costa, S.; Frank, O.; Fridrichová, M.; Vlcková, B.; Vejpravova, J.;

Kalbac, M. SERS of Isotopically Labeled 12C/13C Graphene Bilayer-Gold Nanostructured Film Hybrids: Graphene Layer as Spacer and SERS Probe. *The Journal of Physical Chemistry C* **2017**, *121*, 11680–11686.

(12) Bousige, C.; Balima, F.; Machon, D.; Pinheiro, G. S.; Torres-Dias, A.; Nicolle, J.; Kalita, D.; Bendiab, N.; Marty, L.; Bouchiat, V. et al. Biaxial Strain Transfer in Supported Graphene. *Nano Letters* **2017**, *17*, 21–27.

(13) Alencar, R. S.; Saboia, K. D. A.; Machon, D.; Montagnac, G.; Meunier, V.; Ferreira, O. P.; San-Miguel, A.; Souza Filho, A. G. Atomic-layered MoS 2 on SiO 2 under high pressure: Bimodal adhesion and biaxial strain effects. *Physical Review Materials* **2017**, *1*, 024002.

(14) Francisco-López, A.; Han, B.; Lagarde, D.; Marie, X.; Urbaszek, B.; Robert, C.; Goñi, A. On the impact of the stress situation on the optical properties of WSe_2 monolayers under high pressure. *Papers in Physics* **2019**, *11*, 110005.

(15) Puech, P.; Ghandour, A.; Sapelkin, A.; Tinguely, C.; Flahaut, E.; Dunstan, D. J.; Bacsa, W. Raman G band in double-wall carbon nanotubes combining p doping and high pressure. *Phys. Rev. B* **2008**, *78*, 045413.

(16) Aguiar, A.; Barros, E.; Capaz, R.; Souza Filho, A.; Freire, P.; Filho, J. M.; Machon, D.; Caillier, C.; Kim, Y.; Muramatsu, H. et al. Pressure-induced collapse in double-walled carbon nanotubes: chemical and mechanical screening effects. *J. Phys. Chem. C* **2011**, *115*, 5378–5384.

(17) Barboza, A. P. M.; Guimaraes, M. H. D.; Massote, D. V. P.; Campos, L. C.; Barbosa Neto, N. M.; Cancado, L. G.; Lacerda, R. G.; Chacham, H.; Mazzoni, M. S. C.; Neves, B. R. A. Room-Temperature Compression-Induced Diamondization of Few-Layer Graphene. *Advanced Materials* **2011**, *23*, 3014–3017.

(18) Martins, L. G. P.; Matos, M. J. S.; Paschoal, A. R.; Freire, P. T. C.; Andrade, N. F.; Aguiar, A. L.; Kong, J.; Neves, B. R. A.; de Oliveira, A. B.; Mazzoni, M. S. et al. Raman evidence for pressure-induced formation of diamondene. *Nature Communications* **2017**, *8*, 96.

(19) Filintoglou, K.; Papadopoulos, N.; Arvanitidis, J.; Christofilos, D.; Frank, O.; Kalbac, M.; Parthenios, J.; Kalosakas, G.; Galiotis, C.; Papagelis, K. Raman spectroscopy of graphene at high pressure: Effects of the substrate and the pressure transmitting media. *Phys. Rev. B* **2013**, *88*, 045418.

(20) Machon, D.; Pischedda, V.; Le Floch, S.; San-Miguel, A. Perspective: High pressure transformations in nanomaterials and opportunities in material design. *Journal of Applied Physics* **2018**, *124*, 160902.

(21) Frank, O.; Kavan, L.; Kalbac, M. Carbon isotope labelling in graphene research. *Nanoscale* **2014**, *6*, 6363.

(22) Fang, W.; Hsu, A. L.; Caudillo, R.; Song, Y.; Birdwell, A. G.; Zakar, E.; Kalbac, M.; Dubey, M.; Palacios, T.; Dresselhaus, M. S. et al. Rapid Identification of Stacking Orientation in Isotopically Labeled Chemical-Vapor Grown Bilayer Graphene by Raman Spectroscopy. *Nano Letters* **2013**, *13*, 1541–1548.

(23) Chijioke, A. D.; Nellis, W. J.; Soldatov, A.; Silvera, I. F. The ruby pressure standard to 150GPa. *Journal of Applied Physics* **2005**, *98*, 114905.

(24) Klotz, S.; Chervin, J.-C.; Munsch, P.; Le Marchand, G. Hydrostatic limits of 11 pressure transmitting media. *Journal of Physics D: Applied Physics* **2009**, *42*, 075413.

(25) Finger, L. W.; Hazen, R. M.; Zou, G.; Mao, H. K.; Bell, P. M. Structure and compression of crystalline argon and neon at high pressure and room temperature. *Applied Physics Letters* **1981**, *39*, 892–894.

(26) Vos, W. L.; Schouten, J. A. Improved phase diagram of nitrogen up to 85 kbar. *The Journal of Chemical Physics* **1989**, *91*, 6302–6305.

(27) Mills, R. L.; Olinger, B.; Cromer, D. T. Structures and phase diagrams of N_2 and CO to 13 GPa by x-ray diffraction. *The Journal of Chemical Physics* **1986**, *84*, 2837–2845.

(28) Letoullec, R.; Pinceaux, J. P.; Loubeyre, P. The membrane diamond anvil cell: A new device for generating continuous pressure and temperature variations. *High Pressure Research* **1988**, *1*, 77–90.

(29) Hu, J.; Spain, I. L. Phases of Silicon at High Pressure. *Solid State Communications* **1984**, *51*, 263–266.

(30) Merlen, A.; Bendiab, N.; Toulemonde, P.; Aouizerat, A.; San Miguel, A.; Sauvajol, J. L.; Montagnac, G.; Cardon, H.; Petit, P. Resonant Raman spectroscopy of single-wall carbon nanotubes under pressure. *Phys. Rev. B* **2005**, *72*, 035409.

(31) Jorio, A.; Dresselhaus, M. S.; Saito, R.; Dresselhaus, G. *Raman Spectroscopy in Graphene Related Systems*; Wiley-VCH, 2011.

(32) Decremps, F.; Belliard, L.; Gauthier, M.; Perrin, B. Equation of state, stability, anisotropy and nonlinear elasticity of diamond-cubic (ZB) silicon by phonon imaging at high pressure. *Phys. Rev. B* **2010**, *82*, 104119.

(33) Lee, J. E.; Ahn, G.; Shim, J.; Lee, Y. S.; Ryu, S. Optical separation of mechanical strain from charge doping in graphene. *Nature Communications* **2012**, *3*, 1024.

(34) Mueller, N. S.; Heeg, S.; Alvarez, M. P.; Kusch, P.; Wasserroth, S.; Clark, N.; Schedin, F.; Parthenios, J.; Papagelis, K.; Galiotis, C. et al. Evaluating arbitrary strain configurations and doping in graphene with Raman spectroscopy. *2D Materials* **2017**, *5*, 015016.

(35) Angel, R. J.; Bujak, M.; Zhao, J.; Gatta, G. D.; Jacobsen, S. D. Effective hydrostatic limits of pressure media for high-pressure crystallographic studies. *Journal of Applied Crystallography* **2007**, *40*, 26–32.

(36) Bell, P. M.; Mao, H. K. Degrees of Hydrostaticity in He, Ne, and Ar Pressure-Transmitting Media. *Carnegie Inst. Washington Yearb.* **1981**, *80*, 404 – 406.

(37) Grimsditch, M.; Loubeyre, P.; Polian, A. Brillouin scattering and three-body forces in argon at high pressures. *Physical Review B* **1986**, *33*, 7192–7200.

(38) del Corro, E.; Peña Álvarez, M.; Mračko, M.; Kolman, R.; Kalbáč, M.; Kavan, L.; Frank, O. Graphene under direct compression: Stress effects and interlayer coupling: Graphene under direct compression. *physica status solidi (b)* **2016**, *253*, 2336–2341.

(39) Ferrari, A. C. Raman spectroscopy of graphene and graphite: Disorder, electron-phonon coupling, doping and nonadiabatic effects. *Solid State Communications* **2007**, *143*, 47–57.

(40) Kalbáč, M.; Reina-Cecco, A.; Farhat, H.; Kong, J.; Kavan, L.; Dresselhaus, M. S. The Influence of Strong Electron and Hole Doping on the Raman Intensity of Chemical Vapor-Deposition Graphene. *ACS Nano* **2010**, *4*, 6055–6063.

(41) Lazzeri, M.; Mauri, F. Nonadiabatic Kohn Anomaly in a Doped Graphene Monolayer. *Physical Review Letters* **2006**, *97*, 266407.

(42) Pisana, S.; Lazzeri, M.; Casiraghi, C.; Novoselov, K. S.; Geim, A. K.; Ferrari, A. C.; Mauri, F. Breakdown of the adiabatic Born-Oppenheimer approximation in graphene. *Nature Materials* **2007**, *6*, 198–201.

(43) Das, A.; Pisana, S.; Chakraborty, B.; Piscanec, S.; Saha, S. K.; Waghmare, U. V.; Novoselov, K. S.; Krishnamurthy, H. R.; Geim, A. K.; Ferrari, A. C. et al. Monitoring dopants by Raman scattering in an electrochemically top-gated graphene transistor. *Nature Nanotechnology* **2008**, *3*, 210–215.

(44) Parret, R.; Paillet, M.; Huntzinger, J.-R.; Nakabayashi, D.; Michel, T.; Tiberj, A.; Sauvajol, J.-L.; Zahab, A. A. In Situ Raman Probing of Graphene over a Broad Doping Range upon Rubidium Vapor Exposure. *ACS Nano* **2013**, *7*, 165–173.

(45) Froehlicher, G.; Berciaud, S. Raman spectroscopy of electrochemically gated graphene transistors: Geometrical capacitance, electron-phonon, electron-electron, and electron-defect scattering. *Physical Review B* **2015**, *91*.

(46) Chung, T.-F.; He, R.; Wu, T.-L.; Chen, Y. P. Optical Phonons in Twisted Bilayer Graphene with Gate-Induced Asymmetric Doping. *Nano Letters* **2015**, *15*, 1203–1210.

(47) Lazzeri, M.; Attaccalite, C.; Wirtz, L.; Mauri, F. Impact of the electron-electron correlation on phonon dispersion: Failure of LDA and GGA DFT functionals in graphene and graphite. *Phys. Rev. B* **2008**, *78*, 081406.

(48) Saitta, A. M.; Lazzeri, M.; Calandra, M.; Mauri, F. Giant Nonadiabatic Effects in Layer Metals: Raman Spectra of Intercalated Graphite Explained. *Phys. Rev. Lett.* **2008**, *100*, 226401.

(49) Charles, R. J. Static Fatigue of Glass. I. *Journal of Applied Physics* **1958**, *29*, 1549–1553.

(50) Pinto, H.; Markevich, A. a. J. Electronic and electrochemical doping of graphene by surface adsorbates. *J. Nanotechnol.* **2014**, *5*, 1842–1848.

(51) Kaverzin, A.; Strawbridge, S.; Price, A.; Withers, F.; Savchenko, A.; Horsell, D. Electrochemical doping of graphene with toluene. *Carbon* **2011**, *49*, 3829 – 3834.

(52) Tiberj, A.; Rubio-Roy, M.; Paillet, M.; Huntzinger, J. R.; Landois, P.; Mikolasek, M.; Contreras, S.; Sauvajol, J. L.; Dujardin, E.; Zahab, A. A. Reversible optical doping of graphene. *Scientific Reports* **2013**, *3*, 2355.

(53) Samuels, A. J.; Carey, J. D. Molecular Doping and Band-Gap Opening of Bilayer Graphene. *ACS Nano* **2013**, *7*, 2790–2799, PMID: 23414110.

(54) Proctor, J. E.; Gregoryanz, E.; Novoselov, K. S.; Lotya, M.; Coleman, J. N.; Halsall, M. P. High-pressure Raman spectroscopy of graphene. *Physical Review B* **2009**, *80*.

(55) Sun, Y.; Liu, W.; Hernandez, I.; Gonzalez, J.; Rodriguez, F.; Dunstan, D.; Humphreys, C. 3D Strain in 2D Materials: To What Extent is Monolayer Graphene Graphite? *Physical Review Letters* **2019**, *123*, 135501.

TOC graphic